RESEARCH ARTICLE

Molecular structure and spectroscopic properties of 4-methoxybenzaldehyde based on density functional theory calculations

S. Govindarajan[1], P.B. Nagabalasubramanian[2*]

[1]Department of Physics, Avvaiyar Govt. College for Women, Karaikal-609602.

[2]Department of Physics, Arignar Anna Govt. Arts & Science College, Karaikal-609605.

ABSTRACT: The molecular structure of 4-methoxybenzaldehyde (4MBA) was optimized by the DFT/B3LYP method with 6-311++G(d,p) basis set. The complete vibrational assignment and analysis of the fundamental modes of the compound are carried out using the experimental FTIR and FT-Raman spectra. The stability of the molecule arising from hyper-conjugative interaction and charge delocalization has been studied using NBO and AIM topological analysis. Molecular electrostatic potential, Mulliken and natural atomic charge distributions are calculated. The frontier orbital energy gap and related properties of the molecule illustrates the high reactivity of the title compound. The non-linear optical properties of the compound have been discussed by measuring the dipole moment, the polarizability and hyperpolarizability tensors. Finally, the thermodynamic properties (heat capacity, entropy, and enthalpy) of the title compound at different temperatures were calculated in gas phase.

KEY WORDS: 4-methoxybenzaldehyde; DFT calculations; vibrational analysis; HOMO-LUMO energy gap; NBO and AIM analysis; NLO properties.

1.INTRODUCTION

4-methoxybenzaldehyde compound is widely used in the chemical industry as intermediate in the preparation of perfumes, flavouring agents, dyes, pharmaceuticals, agrochemicals and boiling. The compound consists of a benzene ring with an aldehyde and a methoxy group. Two related isomers ortho-anisaldehyde and meta-anisaldehyde are also known but less commonly encountered. It provides sweet, floral and strong almond odor. The 4MBA, an aromatic aldehyde with methoxy group, is a clear liquid may discolor to yellow on storage (limited shelf life for 6 months) melting at -1 °C, boiling at 249.5 °C insoluble in water, soluble in alcohol and ether.

Ribeiro-Carlo et al. [1] have suggested the existence of dimers in liquid 4MBA based on Raman observations. The title molecule presents several potential donors and acceptors for weak hydrogen bonding. The most efficient hydrogen bond acceptor in the molecule is undoubtedly the carbonyl oxygen atom, but the presence of the acceptor such as the methoxy oxygen and the aromatic π-electron system cannot be ignored. Karger et al. [2] have investigated the formation of C-H···O hydrogen bonded dimers in liquid 4MBA by using ^{1}H and ^{17}O NMR, Raman and FTIR vibrational spectroscopy and ab initio calculations. They showed that most stable dimers have two carbonyl oxygen donors.

So far, Kirchner et al. [3] have determined the crystalline structure of the 4MBA molecule. The 4MBA molecule crystallizes in an orthorhombic space group $P2_12_12_1$, with Z = 4. The unit cell parameters are: a = 4.970 (4) Å, b = 9.043 (9) Å, c = 15.544 (14) A° and $\alpha = \beta = \gamma = 90.0°$. The formyl and methoxy groups lie slightly out of the plane of the benzene ring. The O12-C11-C6-C5 and C2-C3-O14-C15 (see Fig. 2) torsion angles are equal to 4.3 (4) and -2.9 (3), respectively. The C6-C11 bond between aryl and formyl groups, which is found to be 1.455 (3) A°, is slightly shorter than a normal C-C single-bond distance [4]. This is possibly a result of extended conjugation between the aldehyde group and the aromatic ring. Kirchner et al. [3] have showed the formation of several weak C-H···O hydrogen bonds between 4MBA molecules. The distances between hydrogen bond donor and acceptor atoms C···O are in the range of 3.434-3.603 Å.

2.EXPERIMENTAL INFRARED AND RAMAN SPECTRA

The infrared spectrum of the compound under investigation was recorded in the 400-4000 cm^{-1} region at room temperature with a Nicolet model 740 spectrometer, using a globar source, a DTGS detector and KBr cells. The spectra were collected in 32 scans with a resolution of ca. 2 cm^{-1}. The errors in wavenumbers are estimated to be less than 1 cm^{-1}. The Raman spectrum were recorded at room temperature in the same region on a triple monochromator (Jobin Yvon T 64000) using a CCD (Jobin Yvon Spectraview 2D) detector. The liquid samples were sealed in Kimax glass capillaries (i.d. 0.8 mm). The sample was illuminated by the 514.5 nm line of an Ar+ laser (CoherentInova 90) with 50 mW at the sample position. Entry and exit slits of the spectrometer were set to 200 μm, while the slit between premonochromator and spectrograph was opened to 14 mm, giving a resolution of approximately 3 cm^{-1}. The error in wavenumber is estimated to be smaller than 1 cm^{-1}.

3. QUANTUM CHEMICAL CALCULATIONS

DFT has proved to be extremely useful in treating electronic structure of molecules. The B3LYP method based on Becke's three parameter hybrids functional combined with the Lee Yang Parr correlation functional (B3LYP) of DFT yields a

*Corresponding Author: *ekrubha@yahoo.com*

Received: 19.08.2015 **Accepted:** 20.10.2015 **Published on**: 14.12.2015

good definition of harmonic vibrational frequencies for small and medium sized molecules [5,6]. Calculations were carried out with Becke's three parameter hybrid model using the Lee-Yang-Parr correlation functional (B3LYP) method using 6-311++G(d,p) as basis set. All calculations was performed using Gaussian 09W program [7] and GaussView molecular visualization program package [8] with the default convergence criteria without any constraint on the geometry. Molecular geometry of 4MBA was fully optimized by Berny's optimization algorithm using redundant internal coordinates. Harmonic vibrational frequencies were calculated using the analytic second derivatives to confirm the convergence to minima on the potential surface. The optimized geometry of the 4MBA structure no imaginary frequency modes were obtained, therefore there is a true minimum on the potential energy surface was found. The vibrational modes are assigned on the basis of the Total Energy Distribution (TED) analysis using VEDA4 program [9]. GaussView program has been considered to get visual animation and also for the verification of the normal modes assignment.

Table 1. Comparison of calculated geometrical parameters for 4-MBA molecule with the experimental values.

Bond length (Å)	B3LYP	Exp[a]	Bond angle (°)	B3LYP	Exp[a]
C1-C2	1.393	1.383	C2-C1-C6	121.2	122.4
C1-C6	1.396	1.382	C2-C1-H7	119.3	119.3
C1-H7	1.086	0.959	C1-C2-C3	119.2	118.3
C2-C3	1.400	1.394	C1-C2-H8	119.7	120.4
C2-H8	1.081	0.960	C6-C1-H7	119.4	118.4
C3-C4	1.407	1.394	C1-C6-C5	119.0	118.5
C3-O14	1.356	1.357	C1-C6-C11	119.9	119.5
C4-C5	1.379	1.372	C3-C2-H8	121.1	121.3
C4-H9	1.083	0.960	C2-C3-C4	120.1	120.3
C5-C6	1.407	1.401	C2-C3-O14	124.4	124.1
C5-H10	1.084	0.960	C4-C3-O14	115.5	115.5
C6-C11	1.472	1.455	C3-C4-C5	120.1	120.3
C11-O12	1.213	1.214	C3-C4-H9	118.3	119.9
C11-H13	1.111	0.960	C3-O14-C15	119.1	118.0
O14-C15	1.425	1.425	C5-C4-H9	121.6	119.9
C15-H16	1.095	0.970	C4-C5-C6	120.5	120.3
C15-H17	1.088	0.970	C4-C5-H10	120.8	120.4
C15-H18	1.095	0.970	C6-C5-H10	118.7	119.2
			C5-C6-C11	121.1	122.1
			C6-C11-O12	125.3	126.5
			C6-C11-H13	114.4	116.7
			O12-C11-H13	120.3	116.7
			O14-C15-H16	111.3	109.2
			O14-C15-H17	105.7	109.2
			O14-C15-H18	111.3	109.2
			H16-C15-H17	109.4	109.5
			H16-C15-H18	109.7	109.5
			H17-C15-H18	109.4	109.5
RMSD	0.085			1.380	

[a] Experimental values taken from Ref. [3].

The calculated Raman activities (S_i) were suitably converted to relative Raman intensities (I_i) using the following relationship derived from the basic theory of Raman scattering **[10,11]** :

$$I_i = \frac{f(\nu_0 - \nu_i)^4 S_i}{\nu_i \left[1 - \exp(-hc\nu_i / kT)\right]} \quad \ldots \quad (1)$$

Here ν_0 is the laser exciting wavenumber in cm^{-1} (in this work, we have used the excitation wavenumber ν_0= 9398.5 cm^{-1}, which corresponds to the wavelength of 1064 nm of a Nd:YAG laser), ν_i is the vibrational wavenumber of the i^{th} normal mode (cm^{-1}), while S_i is the Raman scattering activity of the normal mode ν_i. f (is a constant equal to 10^{-12}) is a suitably chosen common normalization factor for all peak intensities. h, k, c and T are Planck and Boltzmann constants, speed of light and temperature in Kelvin, respectively. The simulated spectra were plotted using a Lorentzian band shape with a half-width at half-height (HWHH) of 15 cm^{-1}. The electronic properties, such as HOMO–LUMO energies, absorption wavelengths and oscillator strengths were calculated with TD-DFT method at B3LYP/6-311++G(d,p) level.

4. RESULTS AND DISCUSSIONS

4.1. Optimized geometry

Potential energy surface are important because they aid us in visualizing and describing the relationship between potential energy and molecular geometry **[12]**. The conformational analysis was carried out through the potential surface scan in order to ascertain the most stable geometry of 4MBA. The potential energy surface curve was carried out with dihedral angle C4–C3–O14–O15 between methoxy and benzaldehyde group for 4MBA molecule. During the scan, all the geometrical parameters were simultaneously relaxed while the dihedral angle C4–C3–O14–O15 is varied in steps of 36° ranging from 0 to 360°. The curve of the potential energy as a function of the dihedral angle is illustrated in **Fig.1**. Accordingly, there are two local minima observed at 0° or 360° and 180°. From the conformational analysis, the most stable conformer is obtained for 180° torsion angle. Therefore, a detail investigation of this structure will be presented in this work.

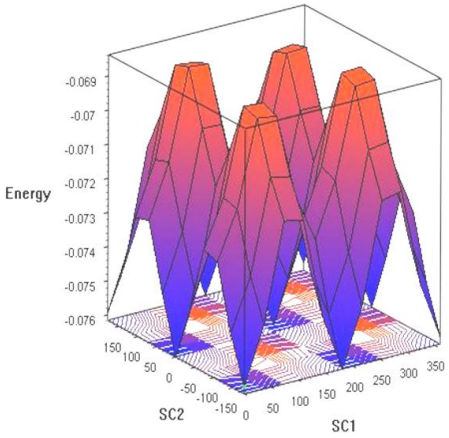

Fig.1. Potential energy scan grid of 4-MBA between SC1 (C3-C4-C14-C15) and SC2 (C2-C1-C11-O12) dihedral angle calculated by AM1 level of theory

For the stable conformer, shown in **Fig.2**, the global minimum energy is -460.22823173 hartrees. In this structure the methoxy and the benzaldehyde group are planar and the methyl group keeps the "trans" position relative to oxygen atom of aldehyde group. The optimized structural parameters of 4MBA calculated by B3LYP/6-311++G(d,p) level of theory are listed in **Table 2**. The optimized computed values of the title compound have been compared with the crystal data in the solid phase at 203 K determined by X-ray diffraction, as published by Kirchner et al. **[3]**. The structural discrepancies between the optimized molecule and crystallographically observed geometry can be analyzed quantitatively by Root Mean Square Deviation (RMSD) overlay. The RMSD fits of the bond lengths and bond angles of experimental and calculated geometries are 0.130 Å and 1.415 Å, respectively, indicating the agreement between the two geometries. From the theoretical values, it is found to that some of the calculated parameters are slightly deviated from the experimental values, due to fact that the theoretical calculations belong to molecule in the gaseous phase and the experimental results belong to molecule in the solid state. The calculated values reproduce reasonable well the experimental bond lengths and angles. The computed C-C bond length varies from 1.393 and 1.472 Å which is in good agreement with experimental data, 1.382–1.455 Å. The slightly deviation is observed for C6-C11 of about 0.017 Å, which may be explained by the formation of C-H…O hydrogen bond between neighboring 4MBA molecules. The calculated C-O bond lengths are in good agreement with the X-ray data. As shown in **Table 1**, the large deviation from the experimental data is observed for C-H bond lengths, which may be explained by the scattering factors of hydrogen atoms in the X-ray diffraction experiment. The calculated bond angles are also in good agreement with the experimental data and the slightly deviation is noted for the O12-C11-H13 and O14-C15-H17 bond angles, which may be explained by the C-H···O hydrogen bonding interaction effects. In **Table 2**, we have given the values of some thermodynamic parameters calculated with B3LYP/6-311++G(d,p) at 298.15 K for 4MBA.

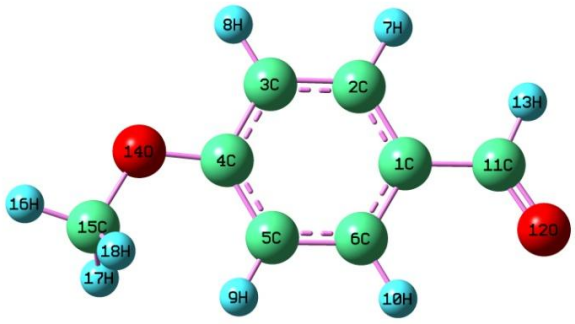

Fig. 2. Optimized molecular structure of 4-MBA along with numbering of atoms

4.2. Molecular electrostatic potential and charge distributions

The molecular electrostatic potential (MEP) provides information for understanding the shape, size, charge density, delocalization and site of chemical reactivity of the molecules **[13,14]**. To predict reactive sites for electrophilic and nucleophilic attack for the title molecule, MEP was calculated at the B3LYP/6-311++G(d,p) optimized geometry

and depicted in **Fig.3**. MEP maps can be obtained by mapping electrostatic potential onto the total electron density with color code. The color code of these maps is in the range between -0.05585 e (deepest red) and -0.05585 e (blue), where blue indicates the strongest attraction and red indicates the strongest repulsion. The negative region is mainly localized on the oxygen atom of the aldehyde group. The more positive region is localized on the hydrogen atoms of the acryl group indicating a possible site for nucleophilic attack. The above results may suggest the formation of intermolecular hydrogen bonding between the two 4MBA molecules.

Table 2. Thermodynamic parameters for 4-MBA obtained by B3LYP/6-311++G(d,p) method.

Parameters	Values
SCF energy (hartree)	-460.2282317
ZPVE (kJ/mol)	371.8695
Rotational constants (GHz)	
A	4.68927
B	0.69431
C	0.60712
Thermal energy (kcal/mol)	94.478
Heat capacity (cal/mol.K)	33.224
Entropy (cal/mol.K)	92.589
Dipole moment (Debye)	5.3329

In addition, the charge distributions over the atoms suggest the formation of donor and acceptor pairs involving the charge transfer in the molecule. The natural and Mulliken atomic charges in 4MBA molecule are calculated and listed in **Table 3**. The Mulliken analysis have showed that the carbon atom C1 exhibit a large negative charge (-0.950752), while the more positive charge is attributed to the carbon atom C6 (0.865473). The natural population analysis have showed that the oxygen atoms O12 (-0.54248) and O14 (-0.53105) present the more negative charges, while the large positive charges are observed for the atoms C3 (0.35377) and C11 (0.41656).

4.3. NBO analysis

NBO analysis is proved to be an efficient method for studying intra- and intermolecular bonding and interactions among bonds, and provides a convenient basis for investigating charge transfer or conjugative interactions in molecular systems **[18]**. The second order Fock matrix was carried out to evaluate the donor-acceptor interactions in the NBO analysis. The interactions result is a loss of occupancy from the localized NBO of the idealized Lewis structure into an empty non-Lewis orbital. For each donor (i) and acceptor (j), the stabilization energy $E^{(2)}$ associated with the delocalization between donor and acceptor is estimated from the second-order perturbation approach **[19]** as given below :

$$E^{(2)} = q_i \frac{F^2(i,j)}{\varepsilon_i - \varepsilon_j} \quad \ldots (2)$$

Table 3. Mulliken and natural atomic charge distributions for 4-MBA calculated by B3LYP/6-311++G(d,p) method

Atoms	Mulliken charges	Natural charges
C1	-0.950752	-0.13636
C2	0.310102	-0.29866
C3	-0.276421	0.35377
C4	-0.598385	-0.23622
C5	0.214235	-0.13277
C6	0.865473	-0.19806
H7	0.159333	0.20654
H8	0.163895	0.21415
H9	0.187636	0.22181
H10	0.196606	0.22767
C11	-0.183978	0.41656
O12	-0.257852	-0.54248
H13	0.122552	0.10113
O14	-0.147132	-0.53105
C15	-0.30604	-0.20684
H16	0.159747	0.17263
H17	0.181233	0.19556
H18	0.159746	0.17263

Table 5. Second order perturbation theory analysis of Fock Matrix in NBO basis of 4-MBA using B3LYP/6-311++G(d,p) method and basis set level calculations.

Donor (i)	Acceptor (j)	E(2)[a]	E(j)-E(i)[b]	F(i,j)[c]
		kJ/mol	a.u.	a.u.
π(C1-C6)	π*(C2-C3)	68.12	0.27	0.06
	π*(C4-C5)	85.29	0.29	0.07
	π*(C11-O12)	91.36	0.28	0.073
π(C2-C3)	π*(C1-C6)	101.74	0.29	0.076
	π*(C4-C5)	57.36	0.3	0.059
π(C4-C5)	π*(C1-C6)	67.62	0.28	0.062
	π*(C2-C3)	96.88	0.27	0.073
LP(2)O12	σ*(C6-C11)	72.56	0.72	0.101
	σ*(C11-H13)	97.26	0.62	0.108
LP(2)O14	π*(C2-C3)	135.61	0.34	0.099
π*(C2-C3)	π*(C1-C6)	1078.65	0.01	0.08
	π*(C4-C5)	573.47	0.02	0.081

[a]$E^{(2)}$ means energy of hyperconjugative interactions(stabilization energy). [b]Energy difference between donor and acceptor i and j NBO orbitals. [c]F(i, j) is the Fock matrix element between i and j NBO orbitals.

Table 6. Charge electron density (ρ) and their Laplacian ($\Delta^2\rho$) at the Bond Critical Point (BCP) calculated using the AIM program (in a.u.).

	C11-O12	C11-H13	C6-C11	C1-C6	C2-H8	C3-O14	O14-C15	C15-H17
ρ	0.388	0.272	0.271	0.305	0.286	0.291	0.242	0.284
$\Delta^2 r$	0.2	-0.922	-0.729	-0.728	-0.956	0.572	-0.376	-0.978

Table 7 . Calculated absorption wavelength (λ), excitation energies (E) and oscillator strengths (f) of 4-MBA molecule using B3LYP/311++G(d,p) method.

		E (eV)	λ (nm)	*f* (a.u)	Major and minor contributions (%)
Gas	1	3.77	328.6	0.0001	HOMO-1 → LUMO (97)
	2	4.69	264.6	0.3374	HOMO → LUMO (82)
	3	4.79	258.7	0.0649	HOMO-2 → LUMO (52), HOMO → LUMO+1 (34)
Methanol	1	3.94	315	0.0002	HOMO-1 → LUMO (97)
	2	4.49	276	0.4919	HOMO → LUMO (95)
	3	4.71	263.3	0.0095	HOMO-2 → LUMO (69), HOMO → LUMO+1 (29)

Table 8. Dipole moment, polarizability and first order hyperpolarizability of 4-MBA obtained by B3LYP/6-311++G(d,p) method

	a.u		a.u
α_{xx}	158.396227	β_{xxx}	1034.81632
α_{xy}	-1.40332984	β_{xxy}	190.213742
α_{yy}	100.637382	β_{xyy}	-47.3775036
α_{xz}	$8.63494070.10^{-5}$	β_{yyy}	107.489871
α_{yz}	$-9.82464287.10^{-5}$	β_{xxz}	$-9.64652831.10^{-4}$
α_{zz}	58.1693855	β_{xyz}	$9.02338248.10^{-4}$
α_{tot}	105.734	β_{yyz}	$-1.87147523.10^{-3}$
$\Delta\alpha$	87.169	β_{xzz}	-34.4682245
μ_x	-1.88106149	β_{yzz}	53.9607825
μ_y	0.92931225	β_{zzz}	$-4.85474138.10^{-3}$
μ_z	$-1.42707480.10^{-5}$	β_0	$1015.7858023 = 8.775 \times 10^{-30}$ esu
μ	2.0981 = 5.3328 Debye		

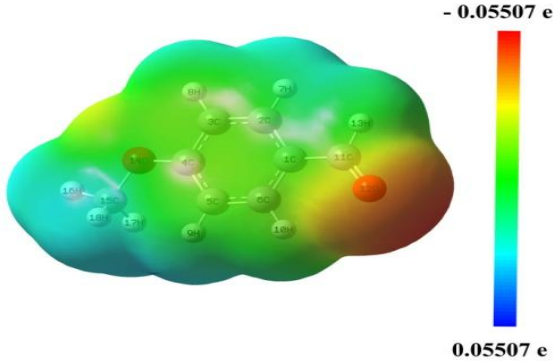

Fig. 3. Molecular electrostatic potential of 4-MBA

Here q_i is the orbital occupancy, ε_i and ε_j are the diagonal elements and F(i,j) is the off-diagonal NBO Fock matrix element. **Table 5** gives the second-order perturbation energy, $E^{(2)}$ corresponding to the interactions and the overlap integral of each orbital pair. From the table, the π electron delocalization in maximum around C1-C6, C2-C3 and C4-C5, distributed to π* antibonding of C11-O12, C1-C6 and C2-C3 with a stabilization energy of about 91.36, 101.74 and 96.88 kJ/mol, respectively. The most important interaction energy, is the electron donation from LP(2)O14 to the antibonding acceptor π*(C2-C3) orbital with the stabilization energy of about 135.61 kJ/mol. The stabilization energy $E^{(2)}$ associated with hyper conjugative interaction LP(2)O12→ σ*(C6-C11) and LP(2)O12→ σ*(C11-H13) are obtained as 72.56 and 97.26 kcal/mol respectively. The interaction energy observed between π* donar and π* acceptor is π*(C2-C3) → π*(C1-C6) and π*(C2-C3) → π*(C4-C5) with stabilization energy of about 1078.65 and 573.47, respectively.

4.4. AIM analysis

The structure of 4MBA has been also studied by using Bader's topological analysis of the charge electron densities (ρ) and their Laplacian ($\nabla^2\rho$) at the Bond Critical Point (BCP) using the AIM program **[20,22]**. The AIM topological parameters ρ and $\nabla^2\rho$ at BCP calculated at B3LYP/6-311++G(d,p) level for the 4MBA molecule are given in **Table 6**. As can be seen in **Table 6**, the value of charge density at the C11-O12 bond critical point is larger and the Laplacian electron density is positive indicating that the electronic charge is depleted between the nuclei. The values of charge density at bond critical points for the benzene ring are relatively high and the $\nabla^2\rho$ is negative. These results indicate that the charge density has been concentrated in the inter-nuclear region.

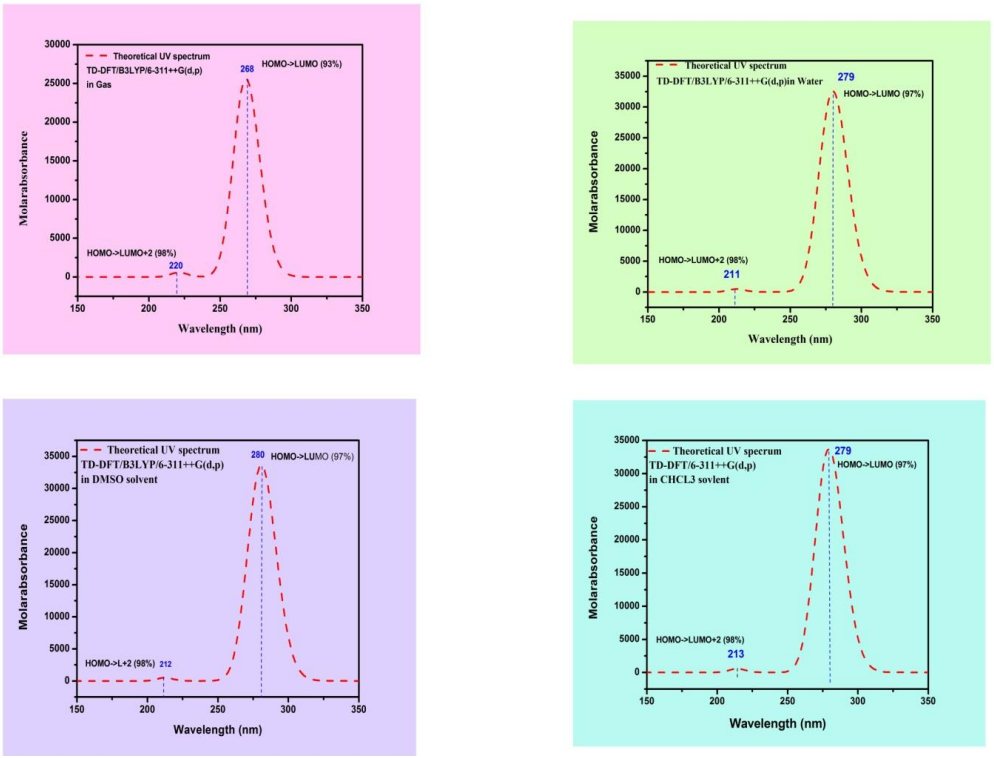

(A)

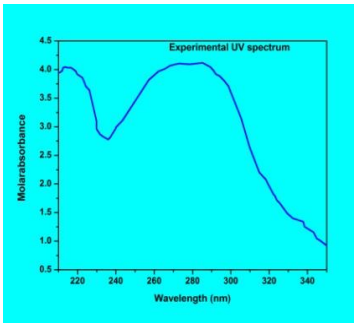

(B)

Fig.4. (A) UV-Vis spectrum of 4-MBA molecue (B) UV-Vis spectrum 4-MBA from NIST

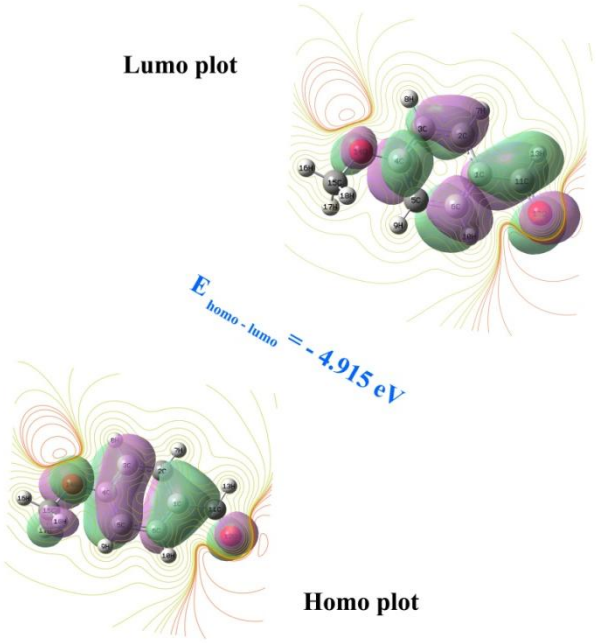

Fig.5. The frontier molecular orbitals HOMO and LUMO of 4-MBA computed with TD-DFT(B3LYP)/6-311++G(d,p) in gas phase

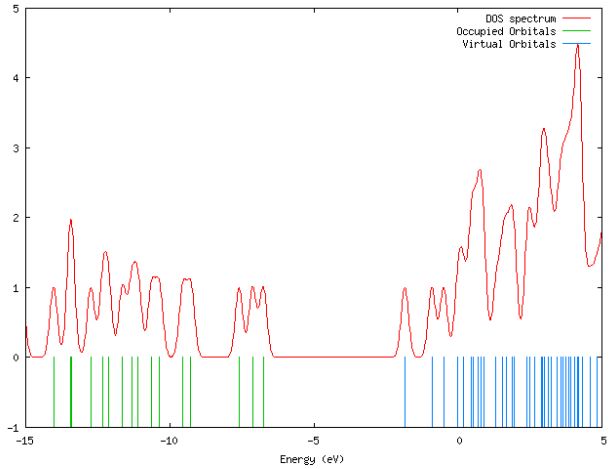

Fig.6. Molecular orbital energy level and density of state (DOS) spectrum of 4MBA molecule

4.5. UV-Vis analysis

To investigate the nature of electronic transitions, the electronic spectra of 4MBA molecule were calculated using the time-dependent density functional theory (TD-DFT) approach at the B3LYP/6-311++G(d,p) level on the basis of fully optimized ground-state structure. Calculations are performed in gas phase and for methanol solvent. The calculated frontier orbital energies, absorption wavelengths (λ), oscillator strengths (*f*) and excitation energies (E) for gas phase and methanol solvent are illustrated in **Table 7**. Oscillator strength is a dimensionless quantity that describes the strength of an electronic transition. Transitions with extremely low or zero *f* values are forbidden.

As can be seen from the **Table 7**, the TD-DFT calculations for the title molecule predict intense electronic transition at 264.6 nm (*f*= 0.3374) in gas phase and 276 nm (*f*= 0.4919) in methanol. The results can, yet, better be represented in graphical form as shown in **Fig.4**. The major contributions of the transitions were designated with the aid of SWizard program **[23]**. Calculations of molecular orbital geometry show that the visible absorption maximum of this molecule corresponds to the electron transition between frontier orbitals such as translation from HOMO to LUMO. This transition is predicted to be of π→π* nature (see **Fig. 5**). The other wavelength, excitation energies, oscillator strength and calculated counterparts with major contributions can be seen in **Table 6**. In **Fig.5**, we have depicted the frontier occupied HOMO and unoccupied LUMO orbital surfaces calculated by TD-B3LYP/6-311++G(d,p) level in gas phase. The positive phase is red and the negative one is green. The HOMO-LUMO energy gap is found to be -4.915 eV. It is worthy to mention that the HOMO is a delocalized π orbital and presents a charge density localized on the methylene group and furan ring expect of oxygen atom. The LUMO is mainly delocalized on the carboxylic and methylene groups.

Gauss-Sum 2.2 program **[24]** has been used to calculate group contributions to the molecular orbitals and prepare the density of the state (DOS) as shown in **Fig.6**. The DOS spectra were created by convoluting the molecular orbital information with gaussian cures of unit height. The HOMO-LUMO energy gap is an important stability index which reflects the chemical stability of the molecule. The lowering of HOMO-LUMO energy gap supports bioactive property of the molecule. It is important to note that for the 4MBA the energy gap is small. Hence it is thermodynamically favorable for an electron transfer to occur. The low value of energy gap is also due to electron withdrawing groups that enter into conjugation.

4.6. Nonlinear optic properties

The nonlinear optic activity provide the key functions for frequency shifting, optical modulation, optical switching and optical logic for the developing technologies in areas such as communication, signal processing and optical interconnections **[15-17]**. The first static hyperpolarizability (β_0) and its related properties (β, α_0 and Δα) have been calculated using DFT-B3LYP/ 6-311++G(d,p) level.

The components of β are defined as the coefficients in the Taylor series expansion of the energy in the external electric field. When the external electric field is weak and homogeneous, this expansion is given below:

$$E = E^\circ - \mu_\alpha F_\alpha - \frac{1}{2}\alpha_{\alpha\beta}F_\alpha F_\beta - \frac{1}{6}\beta_{\alpha\beta\gamma}F_\alpha F_\beta F_\gamma + \ldots (3)$$

Where E° is the energy of the unperturbed molecules, F_α is the field at the origin, μ_α ,$\alpha_{\alpha\beta}$ and $\beta_{\alpha\beta\gamma}$ are the components of dipole moment, polarizability and first hyperpolarizability, respectively. The total static dipole moment, μ, the mean polarizability α_0, the anisotropy of the polarizability Δα and the mean first hyperpolarizability β_0, using the x, y and z components are determined by using the following relations:

$$\mu = (\mu_x^{\,2} + \mu_y^{\,2} + \mu_z^{\,2})^{1/2} \quad \ldots (4)$$

$$\alpha_0 = (\alpha_{xx} + \alpha_{yy} + \alpha_{zz})/3 \quad \ldots (5)$$

$$\Delta\alpha = 2^{-1/2}[(\alpha_{xx}-\alpha_{yy})^2+(\alpha_{yy}-\alpha_{zz})^2+(\alpha_{zz}-\alpha_{xx})^2+6\alpha_{xz}{}^2]^{1/2} \quad (6)$$

$$\beta = ((\beta_{xxx}+\beta_{xyy}+\beta_{zzz})^2+(\beta_{yyy}+\beta_{yzz}+\beta_{yzz})^2+(\beta_{zzz}+\beta_{zxx}+\beta_{zyy})^2)^{1/2} \quad (7)$$

The dipole moment, polarizability and first order hyperpolarizability of the 4MBA are listed in **Table 8**. It is well known that the higher values of dipole moment, molecular polarizability, and hyperpolarizability are important for more active NLO properties.

The calculated dipole moment, polarizability and first order hyperpolarizability of the title molecule are found to be 5.3328 Debye, 15.670×10^{-24} esu and 8.775×10^{-30} esu, respectively. The 4MBA molecule has a dipole moment value larger than the area one, and the first order hyperpolarizability is more than 23 times greater than that of urea (μ and β of urea are 3.8851 Debye and 0.3728×10^{-30} esu). The large value of first order hyperpolarizability is associated with the intramolecular charge transfer, resulting from the electron cloud movement through π conjugated frame work from electron donor to electron acceptor groups. So, we conclude that the present molecule is an attractive object for future studies of nonlinear optical properties.

4.7. Vibrational analysis

The 4MBA molecule possesses C_1 point group symmetry with 48 fundamental normal modes. In the C_1 symmetry, all the fundamental vibrations are active in both FT-IR and FT-Raman spectra. The observed and simulated FT-IR and FT-Raman spectra of 4MBA are shown in **Figs.7&8**, respectively. The observed and scaled theoretical frequencies using DFT/B3LYP with 6-311++G(d,p) basis set with TED are listed in **Table 9**. Calculations were made for a free molecule in vacuum, while experiments were performed for liquid phase. The discrepancies observed between observed and calculated frequencies could be explained due to the fact that the intermolecular interactions unavoidably present in the liquid phase in not taken into account in the gas phase theoretical calculations. The calculated vibrational frequencies were scaled by using SPESCA program **[25]** in order to improve the agreement with the experiment values. So, the calculated harmonic frequencies were scaled by the following straightline: $\upsilon_{scaled} = 0.9527 \times \upsilon_{unscaled} + 16.78$ (with $R^2 = 0.9997$).

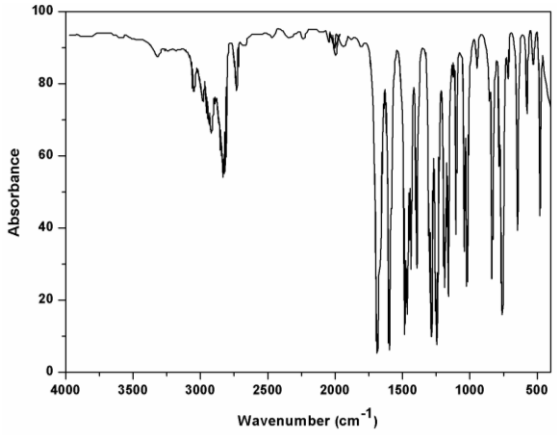

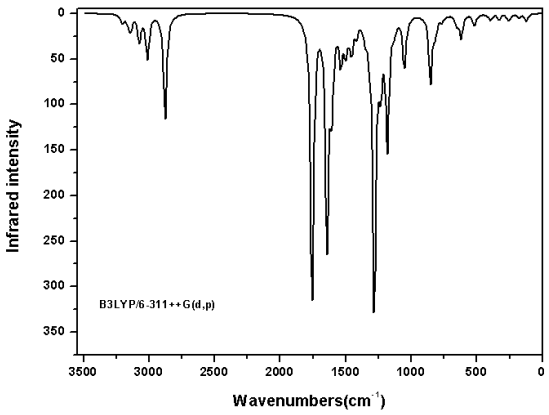

Fig.7. Experimental and calculated (B3LYP/6-311++G(d,p)) FT-IR spectra of 4-MBA

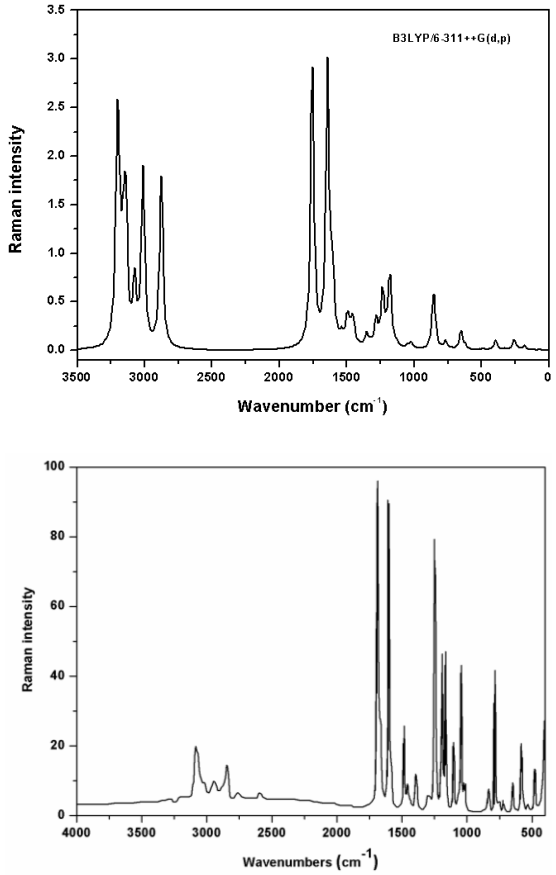

Fig.8. Experimental and calculated (B3LYP/6-311++G(d,p)) FT-Raman spectra of 4-MBA

C-H vibrations. Aromatic compounds commonly exhibit multiple weak bands in the region 3100-3000 cm^{-1} due to aromatic C-H stretching vibration **[26]**. The bands located at 3083 and 3015 cm^{-1} in the infrared spectrum and at 3080 cm^{-1} in the Raman spectrum are assigned to the C-H stretching vibration modes. These bands are predicted at 3072-3027 cm^{-1}. The C-H in-plane bending vibrations are observed in the region from 1300 to 850 cm^{-1} and usually very weak. The bands due to the C-H in-plane vibration

Table 9. Experimental and calculated frequencies (cm-1) using B3LYP/6-311++G(d,p) with percentage of potential energy distribution (PED) of 4-MBA.

Modes	Experimental frequencies		Theoretical frequencies			IR^{int}	R^{int}	Assignments (% PED)[c]
	FT-IR	FT-R	Unscaled	Scaled[a]	Scaled[b]			
1	3083	3080	3207	3121	3072	7.03	72.2	ν_sCHring (97)
2			3200	3114	3065	3.64	95.1	$\nu_s CH_{ring}$ (99)
3			3186	3100	3052	0.33	34.1	$\nu_a CH_{ring}$ (99)
4	3015		3160	3075	3027	7.4	46.6	$\nu_a CH_{ring}$ (97)
5			3142	3057	3010	17.78	87.1	$\nu_a CH_{methyl}$ (91)
6	2947		3075	2992	2946	31.87	37.5	$\nu_a CH_{methyl}$ (100)
7	2848	2847	3013	2932	2887	52.2	100	$\nu_s CH_{methyl}$ (91)
8	2765		2878	2801	2759	127.16	82.9	νC(11)H (99)
9	1689	1689	1757	1710	1691	337.3	20.7	νC(11)O (87)
10	1598		1643	1599	1582	266.33	16.2	νCC_{ring} (44), βHCC (13)
11		1603	1606	1563	1547	94.74	3.29	νCC_{ring} (52), βHCC (11)
12	1484	1487	1539	1497	1483	47.66	0.41	βHCC (46), βCCC (11)
13	1465		1503	1463	1449	29.14	0.34	βHCH_{methyl} (55), τHCOC (24), βHCH (18)
14	1439		1493	1453	1439	10.13	0.88	βHCH_{methyl} (55), βHCH (18), τHCOC (17)
15			1475	1435	1422	5.45	0.28	βHCH_{methyl} (87)
16	1393	1399	1456	1417	1404	35.58	0.97	βHCC_{ring} (23), νCC (15), νCC (13), βHCO (11)
17			1418	1380	1368	16.57	0.07	βHC(11)O (69)
18	1302		1354	1317	1307	15.17	0.4	νCC_{ring} (68)
19	1287		1325	1289	1279	19.48	0.09	βHCC_{ring} (79)
20	1246	1247	1282	1248	1238	345.94	0.64	νCC_{ring} (53)
21	1189	1193	1235	1202	1193	64.12	1.09	νCC(11) (50), βHCC (15)
22	1162	1164	1202	1169	1162	6.17	0.14	τHCOC (62) , βHCH (16)
23			1182	1150	1143	152.54	1.14	βHCC_{ring} (65), νCC (19)
24	1105		1166	1134	1128	0.64	0.07	τHCO(14)C (37), τHCO(14)C (36), βHCH_{methyl} (20)
25	1041	1107	1131	1100	1094	12.46	0.06	βHCC_{ring} (60), νCC (11)
26	1022	1046	1053	1025	1020	59.94	0.03	νO(14)C (73)
27			1026	998	994	1.33	0.04	τH(13)CCC (52), τHCCC (12), τCCCO (13)
28			1021	994	989	0.06	0.02	βCCC_{ring} (81), βHCC (11)
29	950		995	968	965	0.01	0	$\tau HCCC_{ring}$ (70)
30			947	922	919	0.19	0	$\tau HCCC_{ring}$ (68), γOCCC (13)
31			856	833	832	37.58	0.01	νCC_{ring} (66)
32	836		854	830	830	45.25	0	$\tau HCCC_{ring}$ (72), γOCCC (14)
33		787	817	795	795	19.13	0	$\tau HCCC_{ring}$ (76)
34	756		768	747	748	6.62	0	βCCC (30), νCC (15)
35			725	706	707	0.82	0	γO(14)CCC (60), τHCCC (11)

36	650		653	635	639	11.67	0	βCCC (58), νCC (20)
37	582	585	620	603	607	27.73	0	βCCC_{ring} (65)
38	533		520	506	512	14.12	0	τCCCC (66), τHCCC (11)
39	480	482	487	474	481	0.51	0	βCO(14)C (67)
40			431	419	427	0.66	0	$\tau CCCC_{ring}$ (64)
41		406	396	386	394	7.66	0	βCCC (47), νCC (11), νCC (15), βCCC (11)
42			331	322	332	6.97	0	τCCCO (52), τCCCC (12)
43			259	252	264	8.17	0.01	βCCC (66)
44			236	230	242	0.58	0	τHCOC (38), τHCOC (31), τCCCO (13)
45			183	178	191	2.05	0	τCCCO (61), τHCCC (11)
46			178	173	186	2.63	0	βCCC (76)
47			123	120	134	9.35	0	γCCCC (64), τCCCO (15)
48			68	66	82	0	0	τCCCC (65), τCCCC (11)

IR^{int}, infrared intensity (in km/mol); R^{int}, Raman intensity (in A°/amu); ν, stretching; β, in-plane bending; γ, out-of-plane bending; τ, torsion; PED: potential energy distribution.[a]Scaling factor: 0.9731.[b]Frequencies scaled by SPESCA program.[c]PED more than 10% .

coupled with C-C stretching vibrations are observed as a number of sharp medium to weak intensity bands in the 1400–1100 cm^{-1} spectral region. In the present study, the IR bands located at 1393, 1246, 1162 and 1122 cm^{-1} and the Raman bands at 1399, 1247 and 1164 cm^{-1} are assigned to the C-H in-plane bending mode as reported in **Table 9**. These vibrations are calculated at 1404, 1143 and 1094 cm^{-1}. The C-H out-of-plane bending vibrations are strongly coupled vibrations and occur in the region from 950 to 600 cm^{-1} **[27,28]**. The IR bands observed at 836 and 756 cm^{-1} and the Raman bands located at 787 cm^{-1} confirm the presence of C–H out-of-plane bending vibrations, hence agreeing with the values predicted from calculations and reported in literature **[27,28]**. The C-H out-of-plane bending vibrations are predicted at 965, 919, 835 and 795 cm^{-1}.

CH_3 vibrations: The anti-symmetric and symmetric stretching modes of the methyl group generally appear at about 3100 and 2880 cm^{-1}. The bands observed at 2947 cm^{-1} in the IR spectrum and the bands at 2847 cm^{-1} in Raman are assigned to the anti-symmetric stretching mode of the methyl group linked to the O atom. The bands located at 2848 cm^{-1} in the IR spectrum are assigned to the methyl symmetric stretching vibration. The anti-symmetric stretching modes of the methyl group are calculated at 3010 and 2946 cm^{-1}, while the symmetric stretching modes are predicted at 2887 cm^{-1}. The anti-symmetric methyl deformation modes are observed at 1484, 1465, 1439 and 1393 cm^{-1} in the IR spectrum and at 1487 and 1399 cm^{-1} in Raman. The IR bands located at 1439 and 1393 cm^{-1} are assigned to the symmetrical methyl deformation mode. The values reported in literature for these modes are expected in the range 1468–1371 cm^{-1} and the authors do not discriminate between symmetric and anti-symmetric bending modes of the methyl group **[29]**. The IR band located at 1162 cm^{-1} is assigned to the rocking mode.

C-O, C-C and ring vibrations*:* The aromatic carbon–carbon (C=C) stretching vibration occurs in the region 1620–1400 cm^{-1} called ring modes. In the present study, the frequencies observed at 1598, 1484 and 1393 cm^{-1} in the FT-IR spectrum may be assigned to the C=C stretching in the benzene ring. The same vibrations are observed at about 1603, 1487 and 1399 cm^{-1} in the FT-Raman spectrum. The C=C stretching vibrations are calculated at 1582, 1547, 1483, 1404 and 1307 cm^{-1}.

H-C=O vibrations. The C=O stretching vibration of the aldehyde groups give rise to bands at 1725± 65 cm^{-1} **[30-31]**. In this work, the C=O stretching mode of the title compound is observed at 1689 cm^{-1} in the IR and Raman spectra. The C=O stretching mode is predicted at 1688 cm^{-1}. The C-H stretching vibrations give rise to bands in the region 2830–2695 cm^{-1} in aldehyde groups **[31]**. The weak band located at 2765 cm^{-1} in the IR spectrum is assigned to the C(O)-H stretching mode. This band has been predicted at 2759 cm^{-1} by calculations.

4.8. Thermodynamic functions

On the basis of vibrational analysis, the statically thermodynamic functions such as heat capacity at constant pressure ($C°_P$), entropy (S°) and enthalpy changes (ΔH°) for the title molecule were obtained from the theoretical harmonic frequencies using the stand-alone Perl script 'thermo.pl' **[32]** and are listed in **Table 10**. These thermodynamic functions are increasing with temperature ranging from 100 to 1000 K due to the fact that the molecular vibrational intensities increase with temperature **[33]**. The correlation equations between heat capacity, entropy, enthalpy change and temperature were fitted by parabolic formula, and the corresponding fitting factors (R^2) for these thermodynamic properties are 0.99991, 0.99928 and 0.99946, respectively. The corresponding fitting equations are as follows and the correlation graphics of those shows in **Fig. 9**.

Table 10. Thermodynamic properties at different temperatures at the B3LYP/311++G(d,p) level for 4-MBA molecule.

T (K)	S° (J/mol.K)	C_p° (J/mol.K)	H° (kJ/mol)
100.00	279.30	68.700	4.77
200.00	339.39	109.14	13.67
298.15	390.66	150.77	26.41
300.00	391.59	151.56	26.69
400.00	440.95	192.85	43.94
500.00	487.93	228.50	65.06
600.00	532.27	257.80	89.43
700.00	573.87	281.73	116.44
800.00	612.82	301.46	145.63
900.00	649.31	317.91	176.63
1000.00	683.54	331.75	209.13

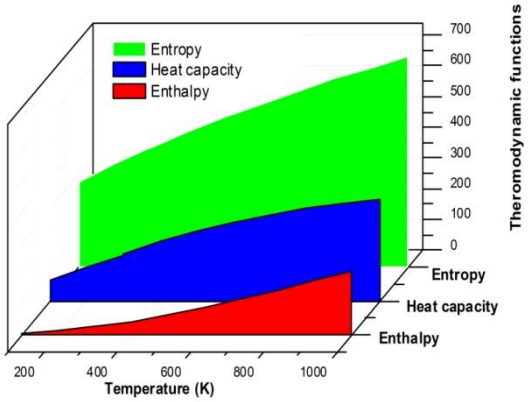

Fig.9. Variation of entropy, heat capacity and enthalpy with temperature for 4-MBA molecule

$$C°_P = 14.08127 + 0.53066\ T - 2.13144 \times 10^{-4}\ T^2$$
$$S° = 222.7817 + 0.6023\ T - 1.42482 \times 10^{-4}\ T^2$$
$$\Delta H° = -5.62454 + 0.0676\ T + 1.49205 \times 10^{-4}\ T^2$$

All the thermodynamic data supply helpful information for the further study on the title molecule. They can be used to compute the other thermodynamic energies according to relationships of thermodynamic functions and estimate directions of chemical reactions according to the second law of thermodynamics in thermo chemical field **[34]**. It is worth to mention that all thermodynamic parameters were computed in gas phase and they could not be used in solution.

5. CONCLUSION

In this work, molecular structure of the 4MBA molecule have been optimized using DFT/B3LYP method using 6-311++G(d,p) basis set. The MEP was calculated to predict the reactive sites for electrophilic and nucleophilic attack for the 4MBA molecule. NBO and AIM analysis reflects the charge transfer within the molecule. HOMO-LUMO energy gap have been determined using TD-DFT calculations. The calculation reveals that the title molecule is an attractive object for future studies of nonlinear optical properties. In addition, on the basis of experimental results and TED calculations, assignments of all the fundamental vibrational frequencies were done. A good correlation between the observed and scaled wave number was obtained for the title compound. Scaled results seemed to be in good agreement with experimental ones. The complete vibrational assignments of wave numbers are made on the basis of total energy distribution (TED). The observed and stimulated spectra are in good agreement with the in DFT/B3LYP/6-311++G(d,p) method. Finally, the variation of thermodynamic functions was reported.

Finally, there has been an increase in facilities capable of manufacturing bicomponent and indeed tricomponent fibres. This not only increases the possibility of having splittable fibres and thereby instantly creating a lot more surface area, but also gives greater potential for creating multicomponent fibres which could potentially have conductive components incorporated into the fibre. Such fibres would find use in applications for either generating or suppressing static electrification.

6. REFERENCES:

1. P.J.A Ribeiro-Claro, L.A.E. Batista de Carvalho, A.M. Amado, J. Raman Spectrosc. 28 (1997) 867.
2. N. Karger, A. M. Amorim da Costa, P.J.A. Ribeiro-Claro, J. Phys. Chem. A 103 (1999) 8672-8677.
3. M.T. Kirchner, D. Bläser, R. Boese, T. S. Thakur, G. R. Desiraju, Acta Cryst. C67 (2011) o387–o390.
4. F.H. Allen, O. Kennard, D.G. Watson, L. Brammer, A. G. Orphen, R. Taylor, J. Chem. Soc. Perkin Trans. 2 (1987) S1-S19.
5. F. Karaboga, U. Soykan, M. Dogruer, B. Ozturk, G. Yildirim, S. Cetin, C. Terzioglu, Spectrochim. Acta Part A 113 (2013) 80.
6. G. Bakalarski, B. Lesyng, Pol. J. Chem. 72 (1998) 1793.
7. M.J. Frisch, G.W. Trucks, H.B. Schlegel, et al., Gaussian 09, Revision B.01, Gaussian, Inc., Wallingford, CT, 2010.
8. R.I. Dennington, T. Keith, J. Millam, GaussView, Version 5.0.8, Semichem. Inc. Shawnee Mission, KS, 2008.
9. M.H. Jamróz, Vibrational Energy Distribution Analysis, VEDA 4, computer program, Poland, 2004.
10. G. Keresztury, Raman spectroscopy theory, in: J.M. Chalmers, P.R. Griffith (Eds.), Handbook of Vibrational Spectroscopy, vol. 1, John Wiley & Sons Ltd., New York, 2002.
11. G. Keresztury, S. Holly, J. Varga, G. Besenyei, A.Y. Wang, J.R. Durig, Spectrochim. Acta 49 (1993) 2007–2026.
12. E.G. Lewars, Computational Chemistry, Springer Science, Bussiness Media, B.V (2011) 1-7.
13. E. Scrocco, J. Tomasi, Adv. Quant. Chem. 11 (1978) 95–115.
14. E.J. Luque, J.M. Lopez, M. Orozco, Theor. Chem. Acc. 103 (2000) 343–350.
15. C. Andraud, T. Brotin, C. Garcia, F. Pelle, P. Goldner, B. Bigot, A. Collet, J. Am. Chem. Soc. 116 (1994) 2094–2101.
16. V.M. Geskin, C. Lambert, J.L. Bredas, J. Am. Chem. Soc. 125 (2003) 15651–15658.
17. D.A. Kleinman, Phys. Rev. 126 (1977) 1962–1979.

18. E.D. Glendening, J.K. Badenhoop, A.D. Reed, J.E. Carpenter, F. Weinhold, NBO 3.1; Theoretical Chemistry Institute, University of Wisconsin, Madison, WI, 1996.
19. J.P. Foster, F. Weinhold, J. Am. Chem. Soc. 102 (1980) 7211–7218.
20. R.F.W. Bader, Atoms in Molecules, A Quantum Theory, Claderon Press, Oxford, 1990.
21. F. Biegler-Köning, J. Schönnbohn, D. Bayles, J. Comput. Chem. 22 (2001) 545.
22. B.F. Minaev, G.V. Baryshnikov, V.A. Minaeva, Dyes Pigment 92 (2011) 531–536.
23. S.I. Gorelsky, SWizard Program Revision 4.5, University of Ottawa, Ottawa, Canada, 2010, <http://www.sg.chem.net/>.
24. N.M. O' Boyle, A.L. tenderholt, K.M. Langer, J. Comput. Chem. 29 (2008) 839–845.
25. M.H. Jamróz, spesca Program, ICRI, Warsaw, 2002.
26. G. Varsanyi.Assignments for Vibrational Spectraof Seven Hundred Benzene Derivatives, Vols. 1 and 2, Academiai Kiado: Budapest, 1973.
27. V. Arjunan, M. Kalaivani, S. Senthikumari, S. Mohan, Spectrochim. Acta A 115, (2013) 154.
28. T.S. Xavier, I. Huber Joe, M.A. Palafox, S. Kumar, V.K. Rastogi, Spectrochim. Acta A 114 (2013) 502.
29. J.G. Rosencrance, P.W. Jagodzinski, Spectrochim. Acta A 42 (1986) 869.
30. M. Kumru, V. Küçük, M. Kocademir, Spectrochim. Acta A 96 (2012) 242.
31. D. Lin-Vien, N.B. Colthup, W.G. Fateley, J.G. Grasselli, The Handbook of Infrared and Raman Characteristic Frequencies of Organic Molecules, Academic Press, 1991 .
32. http://www.nist.gov/mml/csd/informatics_research/thermochemistry_cgi.cfm
33. J. Bevan Ott, J. Boerio-Goates, Calculations from Statistical Thermodynamics, Academic Press, 2000.
34. R. Zhang, B. Dub, G. Sun, Y. Sun, Spectrochim. Acta A 75 (2010) 1115–1124.